Progress in Microbes and Molecular Biology

HH PUBLISHER

Original Research Article

Modulation of Wnt/β-Catenin Signaling Pathway by Bushenfang for Colorectal Tumor Inhibition in mice with Adenomatous Polyposis Coli Gene Mutation

Khang Wen Goh[1], Jie Ji[2*], Xian Gu[3], Rajesh Sreedharan Nair[4], Hemant Kumar Singh Yadav[5], Phei Er Kee[2,6], Siew-Keah Lee[7], Ashok Kumar Janakiraman[8], Long Chiau Ming[9,10], Kai Bin Liew[2*]

Article History

Received: 31 January 2025;

Received in Revised Form: 29 April 2025;

Accepted: 09 May 2025;

Available Online: 31 July 2025

[1]Faculty of Data Science and Information Technology, INTI International University, Persiaran Perdana BBN Putra Nilai, 71800 Nilai, Negeri Sembilan, Malaysia; khangwen.goh@newinti.edu.my (KWG)

[2]Faculty of Pharmacy, University of Cyberjaya. Persiaran Bestari, 63000 Cyberjaya, Selangor, Malaysia

[3]Department of Oncology 5, Longhua Hospital Affiliated to Shanghai University of Traditional Chinese Medicine, 200032 Xuhui District, Shanghai, China; 13761347124@163.com (XG)

[4]School of Pharmacy, University of Nottingham Malaysia, Jalan Broga, 43500 Semenyih, Selangor, Malaysia; Rajesh.Nair@nottingham.edu.my (RSN)

[5]Department of Pharmaceutical Sciences, Indira Gandhi University, Meerpur, Rewari, India; haisunny2@yahoo.co.in (HKSY)

[6]Biorefinery and Bioprocessing Engineering Laboratory, Department of Chemical Engineering and Materials Science, Yuan Ze University, Chungli, Taoyuan 320, Taiwan; pheier.kee@saturn.yzu.edu.tw (PEK)

[7]M. Kandiah Faculty of Medicine and Health Sciences, Universiti Tunku Abdul Rahman, Jalan Sungai Long, Bandar Sungai Long, Kajang 43000, Selangor, Malaysia; leesiewkeah@utar.edu.my (SKL)

[8]Department of Pharmaceutical Technology, Faculty of Pharmaceutical Sciences, UCSI University, Kuala Lumpur, Malaysia; akpharm@gmail.com (AKJ)

[9]Datta Meghe College of Pharmacy, Datta Meghe Institute of Higher Education and Research (deemed to be University), Sawangi (M), Wardha, India

[10]Faculty of Medical and Life Sciences, Sunway University, Sunway City, 47500 Subang Jaya, Selangor, Malaysia; chiaumingl@sunway.edu.my (LCM)

*Corresponding authors: Jie Ji and Kai Bin Liew; Faculty of Pharmacy, University of Cyberjaya. Persiaran Bestari, 63000 Cyberjaya, Selangor, Malaysia ; 2112-4733@st.cyberjaya.edu.my (JJ), liewkaibin@cyberjaya.edu.my (KBL)

Abstract: Colorectal cancer (CRC) remains a major health concern worldwide, with current treatments associated with significant side effects and resistance. Traditional Chinese medicine (TCM), particularly BuShenFang (BSF), has shown potential as an alternative therapeutic strategy. However, the exact mechanism of BSF's action in CRC treatment is not fully understood. Despite the promising anticancer properties of BSF, its mechanism in inhibiting colorectal tumor progression remains unclear, necessitating further investigation. This study aims to evaluate the inhibitory effects of BSF on intestinal adenoma development in APCmin/+ mice and elucidate its underlying mechanism, focusing on the Wnt/β-catenin signaling pathway. APCmin/+ mouse were randomly assigned into four groups: control, low-dose BSF (100 mg/kg), high-dose BSF (200 mg/kg), and xStAxVHLL (positive control). After 11 weeks of treatment, tumor burden, histopathological changes, cell proliferation, apoptosis, and key signaling proteins were assessed using HE staining, immunohistochemistry, TUNEL assay, and Western blot analysis. BSF treatment significantly reduced tumor count and size in a dose-dependent manner. High-dose BSF suppressed tumor cell proliferation, promoted apoptosis, and enhanced APC expression while inhibiting β-catenin accumulation and its downstream targets, including c-Myc, Cyclin D1, and COX-2. These findings suggest that BSF exerts its anti-tumor effects through modulation of the Wnt/β-catenin pathway. BSF demonstrates significant potential in inhibiting colorectal tumorigenesis via modulation of key oncogenic pathways. Further research is warranted to explore its clinical applications and optimize therapeutic dosing.

Keywords: Colorectal cancer; BuShenFang; APCMin/+ mice; Traditional Chinese Medicine; Tumor; SDG 3 Good health and well-being

1. Introduction

BuShenFang (BSF) is a traditional Chinese medicine (TCM) formulation composed of *Pseudobulbus Cremastrae seu Pleiones*, *Fructus akebiae*, *Rehmannia glutinosa*, psoralen, and *Duchesnea indica*, commonly used for kidney tonification. Among these components, *Rehmannia glutinosa* and psoralen are primarily responsible for tonifying the kidneys and spleen, strengthening yang, and enhancing stomach function [1]. In contrast, *Pseudobulbus Cremastrae seu Pleiones*, *Fructus akebiae*, and *Duchesnea indica* contribute to clearing heat, detoxifying the body, resolving carbuncles, and dispersing stagnation [2]. A recent study has suggested that BSF may possess anti-colorectal cancer (CRC) properties, demonstrating significant anti-cancer activity against HCT116 and SW620 CRC cell lines [3]. Nevertheless, the precise mechanisms underlying its anticancer effects have yet to be elucidated. Further investigation into its mechanisms of action and related signaling pathways is crucial to provide a scientific foundation for the clinical application of BSF in colorectal cancer therapy.

It is understood that cells cultured in vitro exist in an environment significantly different from that within a living organism. Tumor cell lines may accumulate impurities or mutations due to excessive transfer or contamination by pathogenic microorganisms, such as mycoplasma, which can compromise the authenticity of experimental results [4]. To enhance the validity and credibility of the research findings, animal model experiments are better options to further verify the results of cell lines study. The dynamic model experiments not only simulate the vivo environment, thereby reducing result uncertainty, but also mitigate potential deviations in experimental outcomes caused by contamination of tumor cell lines [5, 6]. Consequently, to better investigate the relationship between BuShenFang and CRC, multiple mouse groups have been established.

The APC gene is a major tumor suppressor gene located on chromosome 5q21-q22, consisting of 8,535 nucleotides that span 21 exons. Exon 15 is the largest exon, measuring 6571 bp, and accounts for over 75% of the coding region of the gene [7]. The 5' end of the reading frame contains a methionine codon, an in-frame stop codon located 9 bp upstream, and several additional in-frame stop codons at the 3' end. Approximately 10% of the coding region between codons 1286 and 1513 encompasses about 65% of somatic mutations, a region referred to as the "mutation dense region" (MCR), which is situated within exon 15. The APC gene encodes a protein composed of 2843 amino acids, with a molecular weight of approximately 310 kDa [8]. The APC protein is cytoplasmic and hydrophilic, and it is primarily localized on the basement membrane side of colorectal epithelial cells. As cells migrate to the surface of the crypt column, the expression of APC becomes more pronounced. The APC protein features multiple functional domains; the first seventeen amino acids facilitate the formation of homodimers through the establishment of α-helical rods. This region allows the truncated APC protein to interact with the wild-type APC protein. The central portion contains heptavalent repeats (heptad repeat), Armadillo repeats (Am repeats), phosphorylation sites, and a β-Catenin binding site . The C-terminus includes a site responsible for the degradation of β-Catenin and a site that binds to cytoskeletal microtubules. The C-terminus of APC plays a crucial role in cell cycle progression and the regulation of cell growth by interacting with at least three different proteins (EB1, HDLG, and PTP-BL) [9].

Genetic studies utilizing APC mutant mouse models have demonstrated a correlation between mutations in the APC gene and the development of intestinal tumors [10]. When this gene is mutated, it can directly lead to other conditions such as hereditary familial adenomatous polyposis (FAP) and Turcot syndrome, and it is regarded as a 'gatekeeper gene' for colon cancer [11]. The APCmin/+ mouse is a heterozygous gene mutation model, carrying

one normal allele of the *APC* gene and one mutated allele containing a premature stop codon. This mutation leads to early termination of the peptide chain, resulting in a truncated and nonfunctional APC protein. This truncated protein leads to the spontaneous development of intestinal adenomas, which is why these mice are commonly referred to as Min mice [12]. The APCmin/+ model is internationally acknowledged for its heritability, spontaneity, and stability, and is extensively employed in research fields such as cell proliferation, tumor immunity, and the development of anti-cancer therapies.

APC serves as a crucial negative regulator of the classical Wnt signaling pathway, and its permanent inactivation can lead to the activation of this pathway, thereby promoting tumor development. The primary mechanism through which APC inhibits β-catenin/T cell factor (TCF)-dependent transcription is by providing a scaffold for a destruction complex that facilitates the phosphorylation and ubiquitin-dependent degradation of β-catenin. APC enhances the efficiency of this destruction mechanism by promoting Axin multimerization and stabilizing Axin complexes. Additionally, APC prevents the interaction with TCF by directly binding to β-catenin [13]. Conversely, APC negatively regulates β-catenin/TCF transcriptional activity by promoting β-catenin degradation. Loss or mutation of APC leads to β-catenin accumulation, which subsequently activates downstream targets such as Cyclin D1 and c-Myc, influencing cell proliferation, apoptosis, and cell cycle progression [8]. Therefore, APCmin/+ mice represent an ideal animal model for studying intestinal tumors. This study examines the effects of BSF on adenoma growth intervention, adenoma cell proliferation and apoptosis, as well as key molecules in the Wnt/β-catenin signaling pathway in APCmin/+ mice, clarifying its targets and effects within the APCmin/+ mouse model. While XStAxVHLL is a well-known and well-characterized chemical compound used as a positive control. xStAxVHLL is a peptide-based PROTAC (Proteolysis Targeting Chimera) designed to selectively degrade β-catenin, a key protein in the Wnt signaling pathway. It consists of a β-catenin-targeting stapled peptide, xStAx, linked to a VHL-binding peptide, facilitating the recruitment of the von Hippel-Lindau (VHL) E3 ubiquitin ligase. This linkage promotes the ubiquitination and subsequent proteasomal degradation of β-catenin. Two doses of BSF, L-BSF group (100 mg/kg BSF), the H-BSF group (200 mg/kg BSF) were compared to determine whether there is any dose related treatment response. The aim was to further elucidate the mechanism of action of BSF and provide a scientific and theoretical basis for the clinical treatment of CRC.

2. Materials and methods

2.1. Experimental animals

The animal study was conducted at animal research unit, Shanghai Guangde Traditional Chinese Medicine Clinic. SPF grade APCmin/+ mice (Strain number from GemPharmatech Co.: T001457, strain name: APC-mir) were purchased from Gempharmatech Co. Ltd. (Shanghai, China) and raised in a barrier environment maintained at a temperature of 19-22 °C and a relative humidity of 40%-70%. The light cycle was alternated every 12 hours between light and dark, and the mice had free access to food and water. Corncob bedding was replaced every four days. This experiment adhered strictly to the relevant national regulations regarding animal welfare and ethics, with the animal ethics approval number: GD2022A-1 by Ethics Committee of Shanghai Guangde Traditional Chinese Medicine Clinic.

2.2. Main instruments

The main instruments used for sample testing include: biosafety cabinet (sujing antai, Model No. BS-1300IIA2), Super pure water meter (MECK, Model No. Mill-Q Integral5), electronic scales (Mettler Toledo, Model No. ME204E), horizontal shaker (Jiangsu Haimen Qilin Bell instrument, Model No. MICROCL 17), micropipette (GILSON, Model No. KC70239), High current electrophoresis equipment power supply (Bio-Rad, Model No. 1645052), Vertical electrophoresis tank (Bio-Rad, Model No. 1658001), Trough transfer system (Bio-Rad, Model No. 1703930), pH meter (Metter-Toledo GmbH, Germany, Model No. LP115), water bath (Beijing Junyi East Equipment Co., LTD, Model No. JY300), magnetic stirrer (Beijing Junyi East Equipment Co., LTD, Model No. T8-1), microplate spectrophotometer (Biotek, Model No. EPOCH2), centrifugal machine (Thermo, Model No. MICROCL 17), ultrasonic cell disruptor (SONICS, Model No. VCX150), incubator (JINGHONG), Electronic scanner (EPSON, PB4A56180203), Inverted fluorescence Microscope (OLYMPUS, CKX41), Slide and cover slide (Jiangsu Shitai experimental equipment, 10212432C), Shaker (Thermo Fisher Scientific, 10212432C), Palm centrifuge (Shanghai Hengyi Scientific Instrument Co., LTD), 1ml RNase-free bagged tips (EXTRAGENE), 200ul RNase-free bagged tips (EXTRAGENE), 10ul RNase-free bagged tips (EXTRAGENE).

2.3. Main reagents and consumables

The phosphatase inhibitors (Batch No.: S1873), RIPA Lysis buffer (Batch No.: P0013B), BCA protein concentration determination kit (P0010) and Press cassette (5 x 7

inches) (Batch No.: FFC58) were supplied by Beyotime Biotechnology. The PMSF (Batch No.: ST506), SDS (Batch No.: 30166428) and Tris-base (Batch No.: v900483) were supplied by Sigma Sigma (Shanghai) Trading Co., LTD. The TEMED (Batch No.: 17919) and ECL substrate solution (Batch No.: NCI5079) were supplied by Thermo. The HCl (Batch No.: 10011018), glycerinum (Batch No.: 10010618), SDS (Batch No.: 10014118), methanol (Batch No.: 10014118), NACl (Batch No.: 10016318), KCl (Batch No.: 10020318), $Na_2H•12H_2O$ (Batch No.: 10017618), $KHPO_4$ (Batch No.: 10019718) and chloroform (Batch No.: 100006818) were supplied by Sinopharm Group Chemical reagent Co., LTD. The DTT (Batch No.: Amresco0281) and glycine (Batch No.: BL603B) were supplied by Biosharp. The bromophenol blue (Batch No.: BO449-5G), acrylamide (Batch No.: Exp2016109) and Methylacrylamide (Batch No.: Amresc00172) were supplied by Amresco. The Protein marker(14-120KD) (Batch No.: DM111) was supplied by TransGen Biotech. The PVDF membrane (0.45um) (Batch No.: IPVH00010) and PVDF membrane (0.22um) (Batch No.: ISEQ15150) were supplied by Millipore. The developing liquid (Batch No.: 500048-0001), fixative (Batch No.: 500047-0001), isopropanol (Batch No.: A507048), absolute ethyl alcohol (Batch No.: A500737) and DEPC treated water (Batch No.: B501005) were supplied by Sangon Biotech (Shanghai) Co., Ltd. The Crystal violet dye (Batch No.: C0121-500ml), DAPI (Batch No.: C1002) and confining liquid (Batch No.: P0102) were supplied by Beyotime Biotechnology. The Universal Tissue Fixative (neutral) (Batch No.: G1101-500ML) was supplied by Servicebio. The Environmentally friendly dewaxing solution (Batch No.: G1128), Hematoxylin-eosin staining kit (Batch No.: G1076), antifade mounting medium (Batch No.: G1401), EDTA (Batch No.: G1202), diaminobenzidine (DAB) chromogenic reagent for histochemical kit (Batch No.: G1212) were supplied by Xavier Biotechnology Limited. The Neutral balsam (Batch No.: 10004160) was supplied by Sinopharm Group Chemical reagent Co., LTD. The BSA (Batch No.: A600332-0025) was supplied by Sangon Biotech (Shanghai) Co., Ltd. The Tunel (Batch No.: G1501) was supplied by Servicebio. The xStAxVHLL (Batch No.: HY-P5819A) was supplied by MedChemExpress. The APC antibody (Item No.: 19782-1-AP), COX2/Cyclooxygenase 2/PTGS2 antibody (Item No.: 66351-1-Ig), c-Myc antibody (Item No.: 10828-1-AP), GSK3B antibody (Item No.: 22104-1-AP), Cyclin D1 antibody (Item No.: 60186-1-Ig), AXIN1 antibody (Item No.: 16541-1-AP), Beta Catenin antibody (Item No.: 51067-2-AP) and Phospho-GSK3B(Ser9) antibody (Item No.: 67558-1-lg) were purchased from Proteintech Group, Inc. The GAPDH antibody (Item No.: #5174), mouse IgG(HRP) antibody (Item No.: #7076) and rabbit IgG(HRP) antibody (Item No.: #7074) were purchased from Cell Signaling Technology. The Alexa Fluor 488 Labeled Goat Anti-Rabbit IgG antibody (Item No.: GB25303) was purchased from Servicebio.

2.4. Animal grouping and administration mode

Twelve APCmin/+ male mice, aged 4 weeks, were randomly divided into four groups: the L-BSF group (100 mg/kg BSF), the H-BSF group (200 mg/kg BSF), the Ctrl group (control saline group), and the xStAxVHll group (30 mg/kg xStAxVHll positive group), with three mice in each group. The mice weighed between 16 and 20 g and exhibited shiny fur. All mice had unrestricted access to food and water, and their status, diet, and water intake were monitored daily. Weights were recorded weekly. Treatment commenced after a one-week adaptation period. A decoction was prepared using 15 g of shanzi mushroom, 9 g of prezhizi, 15 g of rehmannia glutinosa, 12 g of psoralen, and 15 g of snakeberry, which was diluted in 360 mL of water to achieve a concentration of 183 mg/mL. This solution was further diluted 7.3 times to reach a concentration of 25 mg/mL. For 25g mice, a dosage of 2.5 mg (100 mg/kg) was calculated, equivalent to 100 µL. The L-BSF and H-BSF groups received different concentrations of BSF via gavage once daily at a volume of 0.2 mL, while the Ctrl group administered an equal volume of normal saline. The treatment regimen consisted of intragastric administration five days on and two days off per week for a total duration of 11 weeks. The xStAxVHLL was administered intraperitoneally at a dosage of 30 mg/kg every other day for 13 consecutive days (Figure 1).

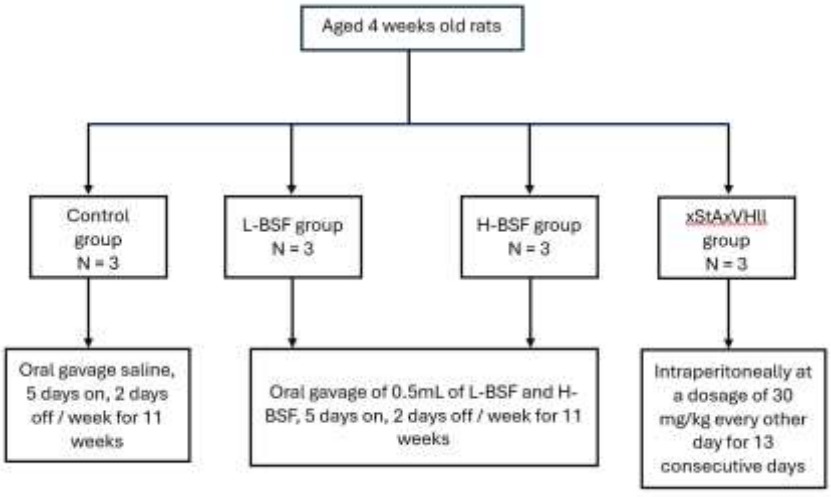

Figure 1. Timeline of the treatment schedule.

2.5. Effect of BSF on intestinal adenomatous polyps in APCmin/+ mice

At the end of 15th week, the mice were sacrificed, and the entire digestive tract was excised. The stomach, small intestine, and colon were separated and thoroughly washed. The small intestine and colon were longitudinally opened and divided into four segments: proximal, middle, and distal small intestine, as well as proximal and distal colon. The number, distribution, and diameter of adenomatous polyps (APs) were assessed using an anatomical

microscope. Following the capture of images of the small intestine and colon tissues, appropriately sized tissue samples were carefully excised, fixed in paraformaldehyde, and subsequently frozen in liquid nitrogen. The inhibition rate of intestinal APs in APCmin/+ mice treated with varying concentrations of BSF was calculated using the formula: [(average number of APs in the control group - average number of APs in the experimental group) / average number of APs in the control group × 100%].

2.6. Observing tissue pathological changes with HE staining

Sample Embedding and Fixation: The tissue was placed in formalin for a 48-hour fixation period. After fixation, the tissue was rinsed with running water to eliminate any residual fixative and impurities. The tissue was stepwise dehydrated with using different concentrations of ethanol: 50%, 70%, 85%, 95%, and finally pure alcohol (absolute ethanol), with each concentration maintained for 2 hours. The tissue could be stored in 70% ethanol for extended periods. Next, the tissue was immersed in a mixture of 50% alcohol and 50% xylene for 2 hours, followed by pure xylene for 2 hours, and then another 2 hours in pure xylene. Subsequently, the tissue block was soaked in a mixture of equal parts molten paraffin and xylene for 1 to 2 hours, before transferring it into two separate containers of molten paraffin for approximately 3 hours each. Once saturated, the wax-soaked tissue block was placed into a container filled with wax liquid, ensuring the tissue block was correctly positioned. After the paraffin solidifies, any excess paraffin surrounding the block was removed in preparation for slicing. Install the slicing knife onto the knife holder of the microtome and secure it tightly. The wax block base was fixed or the wax block itself, adjusting both the wax block and the knife to the appropriate position so that the blade was angled at 5 degrees to the surface of the wax block. Finally, the section thickness were set on the microtome to between 4 and 7 μm, and proceed with sectioning.

Staining: The paraffin sections were dewaxed in water by immersing the sections in environmentally friendly dewaxing solution I for 20 minutes, followed by environmentally friendly dewaxing solution II for another 20 minutes. Next, the sections were subjected to absolute ethanol I for 5 minutes, then absolute ethanol II for 5 minutes, and subsequently 75% alcohol for 5 minutes, concluding with a wash in tap water. The sections were then treated with a high-definition constant stain pretreatment solution for 1 minute. Staining was performed using hematoxylin staining solution for 3-5 minutes, followed by a wash with tap water, differentiation with a differentiation solution, another washed with tap water, a return to blue using a blue-returning solution, and a final rinsed with running water. For eosin staining, the sections were dehydrated in 95% alcohol for 1 minute and stained in eosin

staining solution for 15 seconds. The slices were then placed in absolute ethanol I for 2 minutes, followed by absolute ethanol II for 2 minutes, and absolute ethanol III for 2 minutes. Next, they were treated with n-butanol I for 2 minutes, n-butanol II for 2 minutes, dimethyl I for 2 minutes, and xylene II for 2 minutes to achieve transparency, before being sealed with neutral gum. Finally, microscopic examination, image acquisition, and analysis were conducted.

2.7. Immunohistochemical detection of APC and KI67 levels

Sample Embedding and Fixation: The procedure was the same as described above. Staining: Paraffin sections were sequentially immersed in environmentally friendly dewaxing solution I for 10 minutes, followed by environmentally friendly dewaxing solution II for 10 minutes, and then environmentally friendly dewaxing solution III for 10 minutes. Subsequently, the sections were placed in absolute ethanol I for 5 minutes, absolute ethanol II for 5 minutes, and absolute ethanol III for 5 minutes, after which they were washed with distilled water. The slices were then immersed in a container filled with EDTA antigen retrieval buffer (pH 6.0). Care must be taken to prevent excessive evaporation of the buffer, ensuring that the slices did not dry out. After natural cooling, the slides were placed in PBS (pH 7.4) and shaken on a destaining shaker three times for 5 minutes each. Once the slices were slightly dried, a histochemistry pen was used to draw a circle around the tissue; BSA was added dropwise, and the area was sealed for 30 minutes. The prepared primary antibody APC/KI67 was then added dropwise, and the sections were placed flat in a humidified box for overnight incubation at 4°C. Following this, the slides were washed three times with PBS (pH 7.4) while shaking on a destaining shaker for 5 minutes each time. A secondary antibody was added, and the slides were incubated at room temperature for 50 minutes in the dark. The slides were then washed again three times with PBS (pH 7.4) while shaking for 5 minutes each time. After the slices were slightly dried, freshly prepared DAB chromogenic solution was added dropwise within the drawn circle. The color development time was monitored under a microscope, with positive color indicated by a brown hue. Finally, the slices were rinsed with tap water to halt the color development.

2.8. TUNEL detects tissue apoptosis

Dewax paraffin sections to water: The sections were placed in xylene I for 10 minutes, followed by xylene II for 10 minutes, and repeated xylene II for another 10 minutes. Then proceed with absolute ethanol I for 5 minutes, absolute ethanol II for 5 minutes, and absolute ethanol III for 5 minutes, concluding with a wash using distilled water. (Note: The dewaxing time may need to be extended during winter.)

Proteinase K treatment: After the sections were slightly dried, use a histochemistry pen to draw a circle around the tissue to prevent the liquid from flowing away. The drops of the proteinase K working solution within the circle was added to cover the tissue, and incubated at 37°C for 22 minutes. Subsequently, the slides were placed in PBS (pH 7.4) and shaked on a destaining shaker three times for 5 minutes each. (Preparation method for proteinase K working solution: original solution: PBS = 1:9.)

Membrane rupture: Once the slices were slightly dried, the membrane rupture working solution within the circle was applied to cover the tissue, incubated at room temperature for 20 minutes, and then washed the slides in PBS (pH 7.4) by shaking three times for 5 minutes each on a decolorizing shaker.

Equilibrate at room temperature: After the slices were slightly dried, buffer dropwise within the circle was added to cover the tissue, and incubated at room temperature for 10 minutes.

Add reaction solution: Based on the number of slices and tissue size, an appropriate amount of TDT enzyme was prepared, dUTP, and buffer from the TUNEL kit. Mix in a 1:5:50 ratio, apply to the circle to cover the tissue, and the slices flat was placed in a humidified box. Incubate in a 37°C incubator for 2 hours, ensuring to add a small amount of water to the humidified box to maintain humidity.

DAPI counterstaining of cell nuclei: The sections were rinsed with PBS (pH 7.4) three times for 5 minutes each. After removing the PBS, DAPI dye solution was applied to the designated area and incubated at room temperature for 10 minutes in the dark.

Sealing the slides: The slides were placed in PBS (pH 7.4) and gently agitated them on a destaining shaker three times for 5 minutes each. The sections should then be lightly shaken to remove excess liquid and mounted using an anti-fluorescence quenching mounting medium.

Microscopic examination and photography: The sections were examined under a fluorescence microscope and captured images. (DAPI has a UV excitation wavelength of 330-380 nm, an emission wavelength of 420 nm, and emits blue light; FITC has an excitation wavelength of 465-495 nm, an emission wavelength of 515-575 nm, and emits green light).

2.9. Immunofluorescence (IF) detects the nuclear entry of β-catenin

Sample Embedding and Fixation: The procedure was the same as described above. Staining procedure: The paraffin sections were immersed in environmentally friendly dewaxing liquid I for 10 minutes, followed by environmentally friendly dewaxing liquid II for another 10 minutes, and then environmentally friendly dewaxing liquid III for an additional 10 minutes. Subsequently, the sections were treated with absolute ethanol I for 5 minutes, absoluted ethanol II for 5 minutes, and absoluted ethanol III for 5 minutes, followed by washing with distilled water. The slices were placed in a container with EDTA antigen retrieval buffer (pH 6.0), ensuring that excessive evaporation of the buffer was prevented and that the slices remained moist. After allowing the sections to cool naturally, the slides was transfered to PBS (pH 7.4) and shaked them on a destaining shaker for three intervals of 5 minutes each. Once the slices were slightly dried, a histochemistry pen was used to outline the tissue, then BSA was dropwise added and sealed for 30 minutes. Next, the prepared primary antibody was dropwise added, and the sections were flat incubated in a humidified box overnight at 4°C. After incubation, the slides were washed in PBS (pH 7.4) three times with shaking on a destaining shaker for 5 minutes each. Following this, the corresponding secondary antibody (diluted 1:500) was applied and incubated at room temperature for 50 minutes in the dark. The slides were washed again in PBS (pH 7.4) three times with shaking on a destaining shaker for 5 minutes each. Finally, DAPI dye solution was added and incubated at room temperature for 10 minutes in the dark. The slides was washed three times in PBS (pH 7.4) on a destaining shaker for 5 minutes each, and then mount with an anti-fluorescence quenching mounting medium before viewing under a microscope.

2.10. Western Blot Analysis of Downstream Protein Levels in the Wnt/β-Catenin Signaling Pathway

Tissue Sample Preparation: An appropriate amount of target tissue was placed into a 1.5 mL grinding tube. A suitable volume of lysis solution was added and incubated on ice for 30 minutes. Subsequently, transfer the mixture to a grinder and visually assess the degree of tissue grinding. An ultrasonic crusher was utilized to sonicate each sample in an ice bath at 25% power for one second, followed by a one-second interval, and repeated this cycle 10 times. It was crucial to perform this operation on ice to prevent protein degradation. After sonication, the samples were centrifuged to sediment cell debris (4°C, 13,000 rpm, for 10 minutes) and carefully transfered the supernatant to a new tube for subsequent steps, avoiding any lipids that might float on the surface of the supernatant during transfer.

Determination of Protein Concentration: The protein sample was appropriately diluted by mixing 4 μL of each sample with 16 μL of PBS, resulting in a five-fold dilution. Bradford standards were prepared to create tissue protein concentrations of 0.00, 0.125, 0.25, 0.5, 0.75, 1.00, and 1.5 mg/mL. The protein standards of varying concentrations were added to the designated wells of a 96-well plate and included two parallel wells of PBS as blank controls. Ensure that the total sample volume in each well was 5 μL. Then, 250 μL of G250 staining solution was added to each well, taking care to avoid bubble formation, which could interfere with the reaction. Absorbance could be measured immediately or within 2 hours; however, detection data might not be reliable if assessed beyond this timeframe. The linear regression equation was calculated by basing on the standard protein concentrations and their corresponding OD values, and using this regression equation to determine the protein concentration of the samples based on their OD values.

Protein Denaturation: The extracted protein was supernatant combined with 5× protein loading buffer and incubated in a boiling water bath for 10 minutes. Preparation of SDS-PAGE Gel: After the glass plates were thoroughly cleaned and dried, secured them in the gel maker. Begin the separation gel was prepared by pouring it into the gap between the glass plates to an appropriate height, then covered it with absolute ethanol. The gel was allowed to polymerize completely. Once polymerization was complete, the absolute ethanol was discarded , the gel was gently rinsed with double-distilled water, and blotted it dry using filter paper. Subsequently, the stacking gel was added to the appropriate height and inserted the comb. After the stacking gel was fully polymerized, the comb was carefully removed. Preparation of separation gels of various concentrations:8%, 10%, 12% and 15% separation glue.

Electrophoresis Separation: The prepared gel was secured within the electrophoresis tank and poured the electrophoresis solution into the storage tank. Using a micropipette, the prepared protein sample was added and marker to the loading well, ensuring that the total protein amount for each sample was 20 μg. After sample addition, electrophoresis at a constant voltage of 80 V was initiated until the bromophenol blue indicator formed a distinct line at the interface of the stacking gel and the separation gel. Subsequently, the voltage increased to a constant 100 V until the bromophenol blue reached the bottom of the gel. This process typically requires approximately 1.5 hours.

Electrotransfer: The gel was carefully removed and excised the band of interest based on the marker. The band was rinsed with distilled water, then the PVDF membrane was cut and filter paper to match the dimensions of the PAGE gel. The PVDF membrane was soaked

in methanol for a few seconds, followed by soaking both the membrane and filter paper in the electrotransfer buffer. The layers were assembled in the following order: black plate, fiber pad, filter paper, gel, PVDF membrane, filter paper, fiber pad, and white plate. The clamps were secured and placed into the film transfer instrument, ensuring that one side of the black plate aligned with the black negative electrode. The transfer tank was filled with electrotransfer solution and initiated the transfer process under the following conditions: 100 V constant voltage in an ice bath for 60 minutes.

To initiate immunoblot color development, the PVDF membrane was immersed in TBST (blocking solution) containing 5% skimmed milk powder and blocked it on a shaker at room temperature for 40 minutes. Subsequently, the corresponding primary antibody was diluted with using the primary antibody diluent, and incubated the PVDF membrane in this primary antibody solution at 4°C overnight. Following this incubation, the PVDF membrane was thoroughly washed with TBST three times, allowing 5 minutes per wash. Next, the corresponding HRP-labeled secondary antibody was diluted in TBST at a ratio of 1:20,000, and incubated the PVDF membrane in the secondary antibody solution on a shaking table at 37°C for 1 hour. After this incubation, washed the membrane thoroughly with TBST three times, again allowing for 5 minutes per wash. The working solution by mixing the enhancer solution was prepared and the stable peroxidase solution from the ECL reagent in a 1:1 ratio. This working solution was applied to the PVDF membrane and allow it to react for a few minutes until the fluorescent band becomes visible. Subsequently, filter paper was used to absorb any excess substrate solution. Finally, the membrane was covered with cling film, the X-ray film was pressed onto it, and placed it into the developer solution for development, followed by the fixer solution for fixation. The film was developed.

2.11. Statistical analysis

The experimental data were analyzed using SPSS version 27.0 statistical software, while GraphPad Prism version 9.0 was utilized for graphical representation. The experimental data are expressed as mean ± standard deviation (x ± SD). Independent samples t-test was used to determine whether there is a significant difference between two groups. One-way analysis of variance (ANOVA) was employed for comparisons of more than 2 groups to determine statistically significant differences. Post-hoc Dunnet's test was used to compare groups with the control group when there is a significant difference. A p-value of 0.05 was considered statistically significant, among which * vs Ctrl $p < 0.05$, ** vs Ctrl $p < 0.01$, *** vs Ctrl $p < 0.001$, # vs xStAxVHLL $p < 0.05$, ## vs xStAxVHLL $p < 0.01$, ### vs xStAxVHLL $p < 0.001$.

3. Results

3.1. BSF inhibits the number of intestinal APs in APCmin/+ mice

APCmin/+ mice model was used in this study, which can spontaneously develop multiple polypoidal adenomas due to a heterozygous mutation in the APC gene at position 850. This mutation results in the continuous activation of the Wnt/β-catenin signaling pathway, leading to the early development of CRC, which closely resembles human CRC in terms of surface characteristics. Consequently, APCmin/+ mice are extensively utilized as animal models for CRC. BSF was administered at doses of 100 mg/kg and 200 mg/kg to the mice in the L-BSF and H-BSF groups, respectively, five days a week with two days off, over a total duration of 11 weeks. Additionally, xStAxVHLL was given intraperitoneally at a dose of 30 mg/kg every other day for 13 consecutive days. Concurrently, mice in the Ctrl group received the same volume of physiological saline. Following treatment, tumors were observed in both the small intestine (Figure 2) and colon (Figure 3) of the APCmin/+ mice, with a higher incidence of tumors in the colon. Notably, as the concentration of BSF increased, there was a sequential decrease in both the overall number and size of tumors in the small intestine and colon. Specifically, the L-BSF group exhibited a 53.33% inhibition of adenomatous polyps (APs), the H-BSF group showed a 66.67% inhibition, and the xStAxVHLL group demonstrated a 46.67% inhibition (Figure 4). These findings indicate that the inhibition of intestinal APs in mice correlates positively with increasing concentrations of BSF.

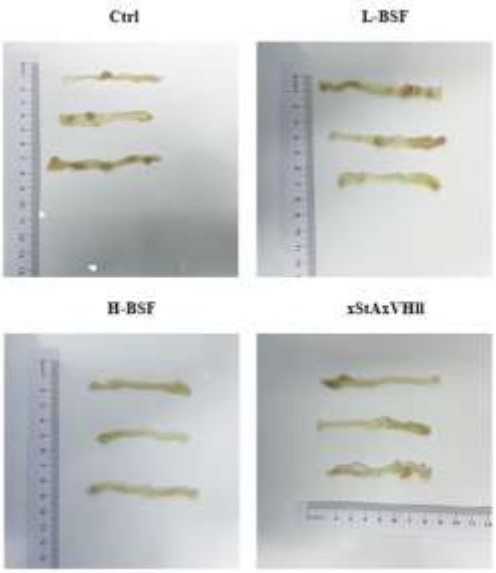

Figure 2. The effect of BSF on small intestinal adenomas in APCmin/+ mice. Ctrl indicates the control group, L-BSF represents a low dose of BSF (100 mg/kg), H-BSF denotes a high dose of BSF (200 mg/kg), and xStAxVHLL serves as the positive control.

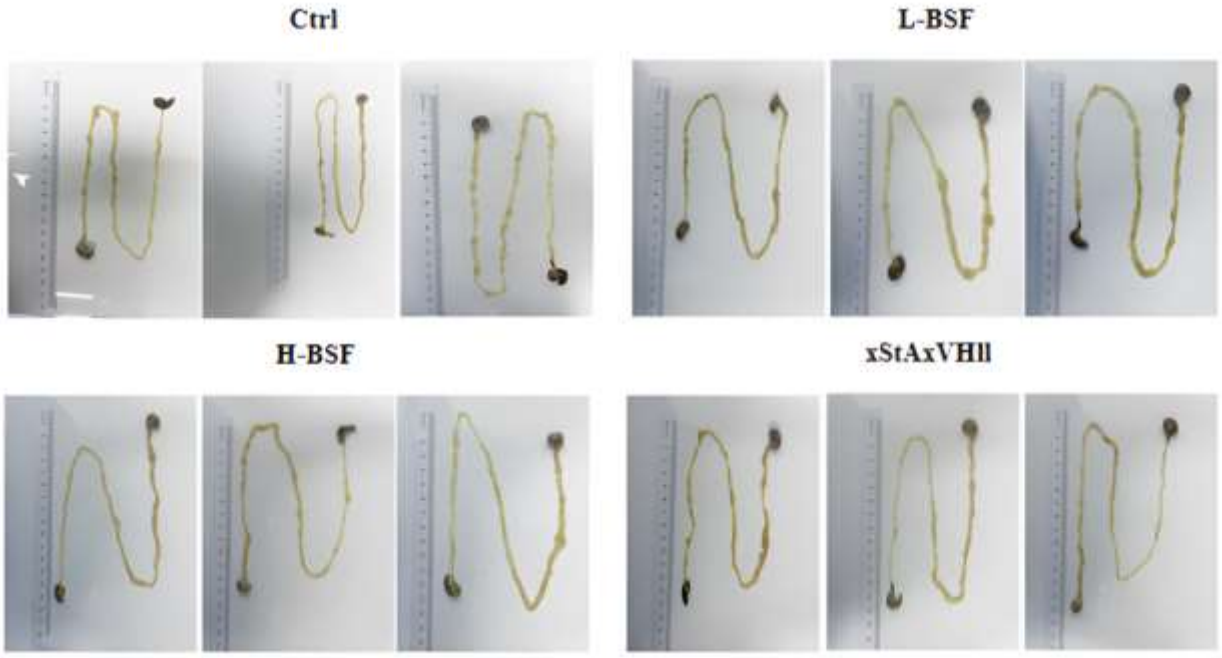

Figure 3. The effect of BSF on colon adenomas in APCmin/+ mice. Ctrl indicates the control group, L-BSF represents a low dose of BSF (100 mg/kg), H-BSF denotes a high dose of BSF (200 mg/kg), and xStAxVHLL serves as the positive control.

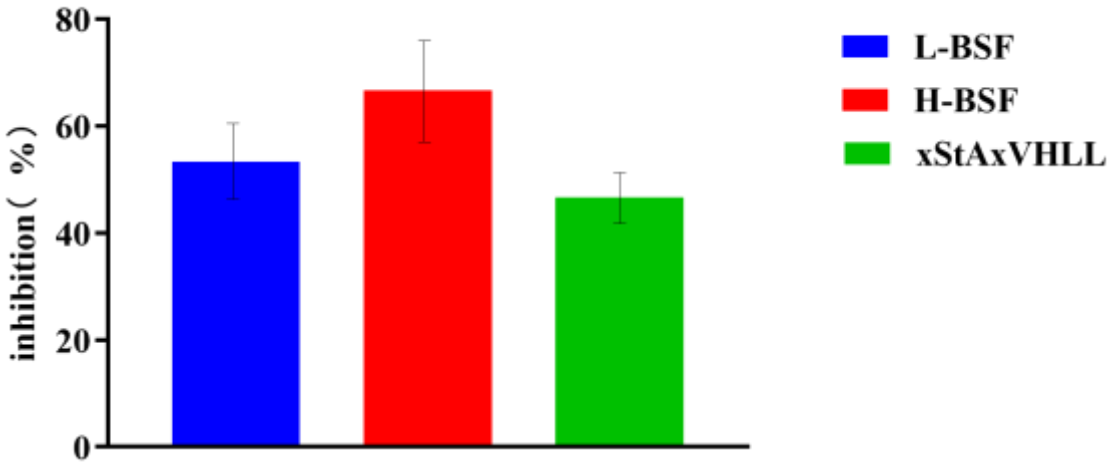

Figure 4. The effect of BSF on the number of intestinal APs in APCmin/+ mice. L-BSF represents a low dose of BSF (100 mg/kg), H-BSF denotes a high dose of BSF (200 mg/kg), and xStAxVHLL serves as the positive control.

3.2. BSF inhibits the carcinogenesis of intestinal tumors in APCmin/+ mice

Pathological changes in the intestinal tissue were examined using HE staining, revealing notable canceration in the intestinal tissue of both the Ctrl group and the L-BSF group. In contrast, significant improvements were observed in the H-BSF group and the xStAxVHLL group (Figure 5). These findings suggest that BSF alleviates the canceration of intestinal adenomas in APCmin/+ mice.

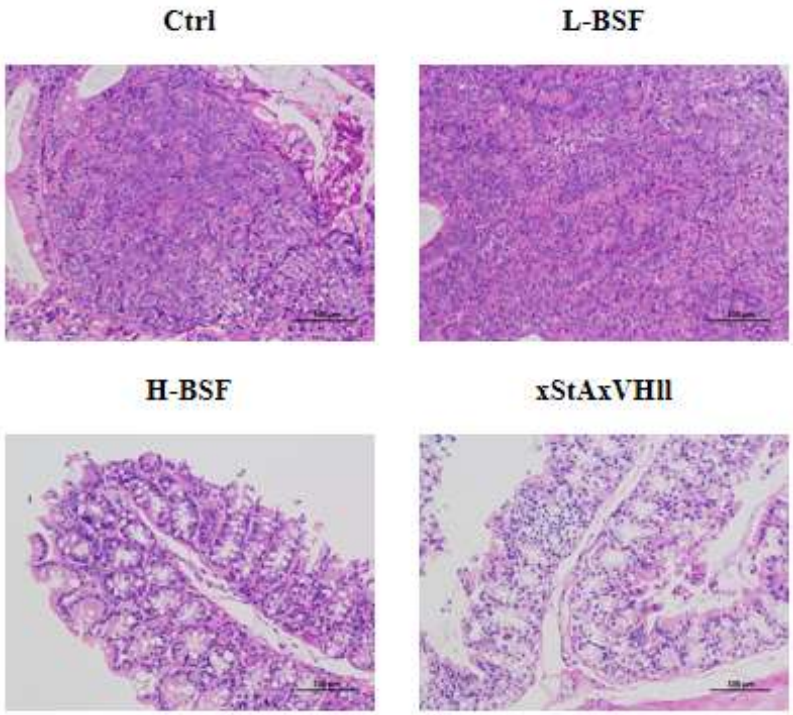

Figure 5. Effect of BSF on intestinal tumor histopathology in APCmin/+ mice (100X). Ctrl indicates the control group, L-BSF represents a low dose of BSF (100 mg/kg), H-BSF denotes a high dose of BSF (200 mg/kg), and xStAxVHLL serves as the positive control.

3.3. BSF inhibits the proliferation of intestinal tumor cells in APCmin/+ mice

To investigate the effect of BSF on the proliferation of intestinal adenoma tumor cells, the degree of cell proliferation in intestinal tumor tissues was assessed. Immunohistochemistry results indicated no significant changes in the Ctrl and L-BSF groups. In contrast, the expression of KI67 was reduced in the H-BSF and xStAxVHLL groups compared to the Ctrl and L-BSF groups. These findings suggest that high doses of BSF can effectively inhibit the proliferation of intestinal tumor cells (Figure 6).

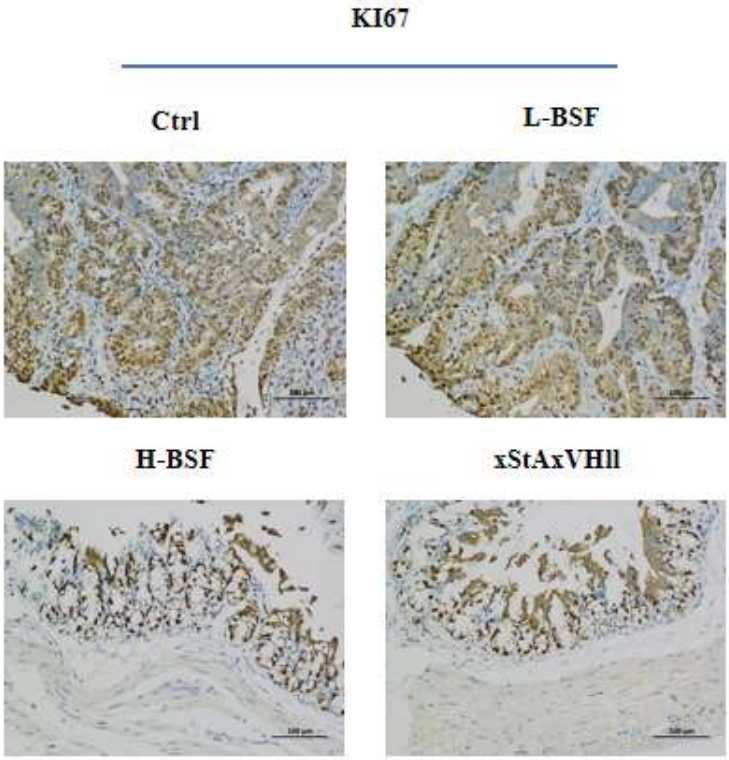

Figure 6. Effect of BSF on intestinal KI67 expression in APCmin/+ mice (100X). Ctrl indicates the control group, L-BSF represents a low dose of BSF (100 mg/kg), H-BSF denotes a high dose of BSF (200 mg/kg), and xStAxVHLL serves as the positive control.

3.4. BSF promotes apoptosis of intestinal tumor cells in APCmin/+ mice

TUNEL staining was utilized to assess the effects of varying concentrations of BSF and xStAxVHLL on apoptosis in APCmin/+ mice. The results presented in Figure 7 indicate that, in comparison to the Ctrl group, cell apoptosis was significantly increased in both the L-BSF and H-BSF groups, as well as in the xStAxVHLL group. These findings suggest that BSF effectively promotes the apoptosis of intestinal tumor cells.

3.5. BSF enhances the expression of APC in the intestinal tissue of APCmin/+ mice

Immunohistochemistry was employed to evaluate APC levels in intestinal tumor tissues. The results revealed no significant changes in the Ctrl and L-BSF groups. However, APC expression was notably elevated in the H-BSF and xStAxVHLL groups when compared to both the Ctrl and L-BSF groups (Figure 8). Therefore, high doses of BSF are associated with increased APC levels in the intestinal tissues of APCmin/+ mice.

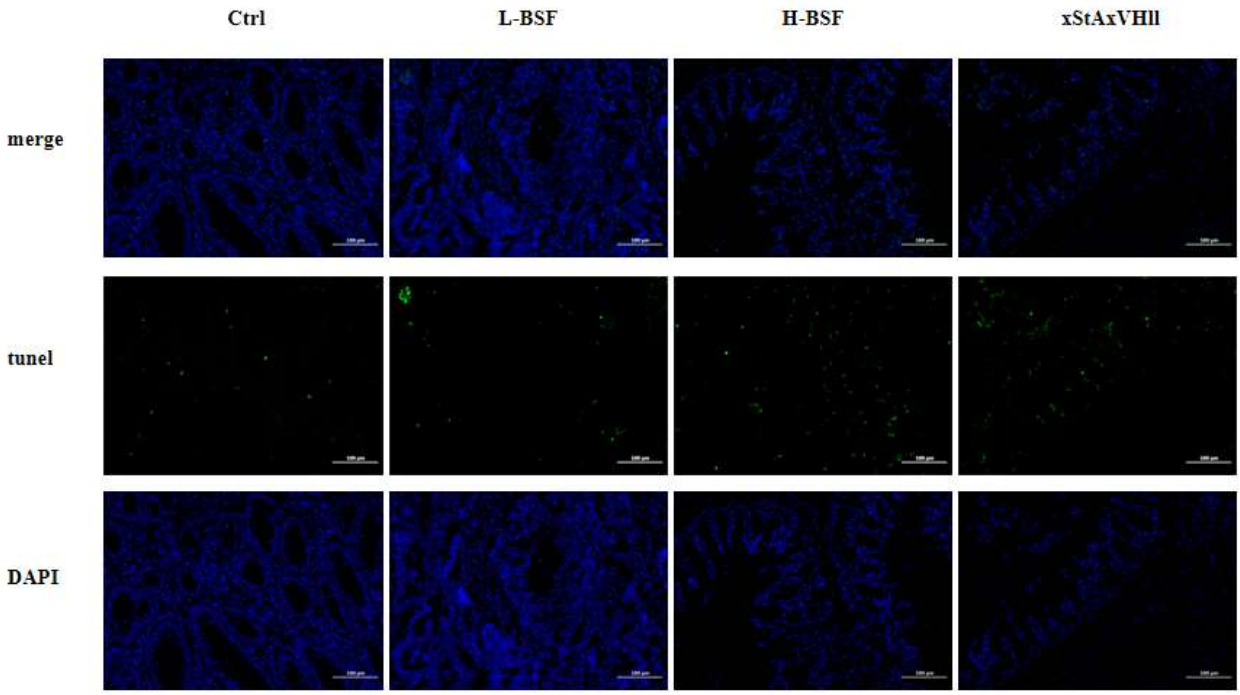

Figure 7. The effect of BSF on the apoptosis of intestinal tumor cells in APCmin/+ mice (100X). Ctrl indicates the control group, L-BSF represents a low dose of BSF (100 mg/kg), H-BSF denotes a high dose of BSF (200 mg/kg), and xStAxVHLL serves as the positive control.

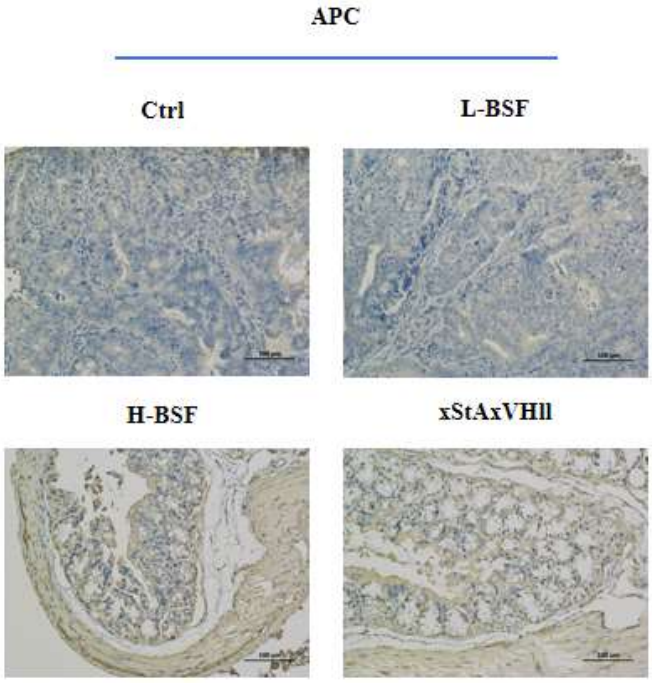

Figure 8. The effect of BuShenFang on the expression of APC in the intestine of APCmin/+ mice. Ctrl indicates the control group, L-BSF represents a low dose of BSF (100 mg/kg), H-BSF denotes a high dose of BSF (200 mg/kg), and xStAxVHLL serves as the positive control.

3.6. BSF inhibits the expression of β-catenin in the intestinal tissue of APCmin/+ mice

Concurrently, immunofluorescence results demonstrated that, in the intestinal tissue of APCmin/+ mice, the expression of β-catenin sequentially decreased in the L-BSF, H-BSF, and xStAxVHLL groups when compared to the Ctrl group (Figure 9). These findings robustly support the conclusion that BSF can downregulate β-catenin protein levels in vivo in APCmin/+ mice.

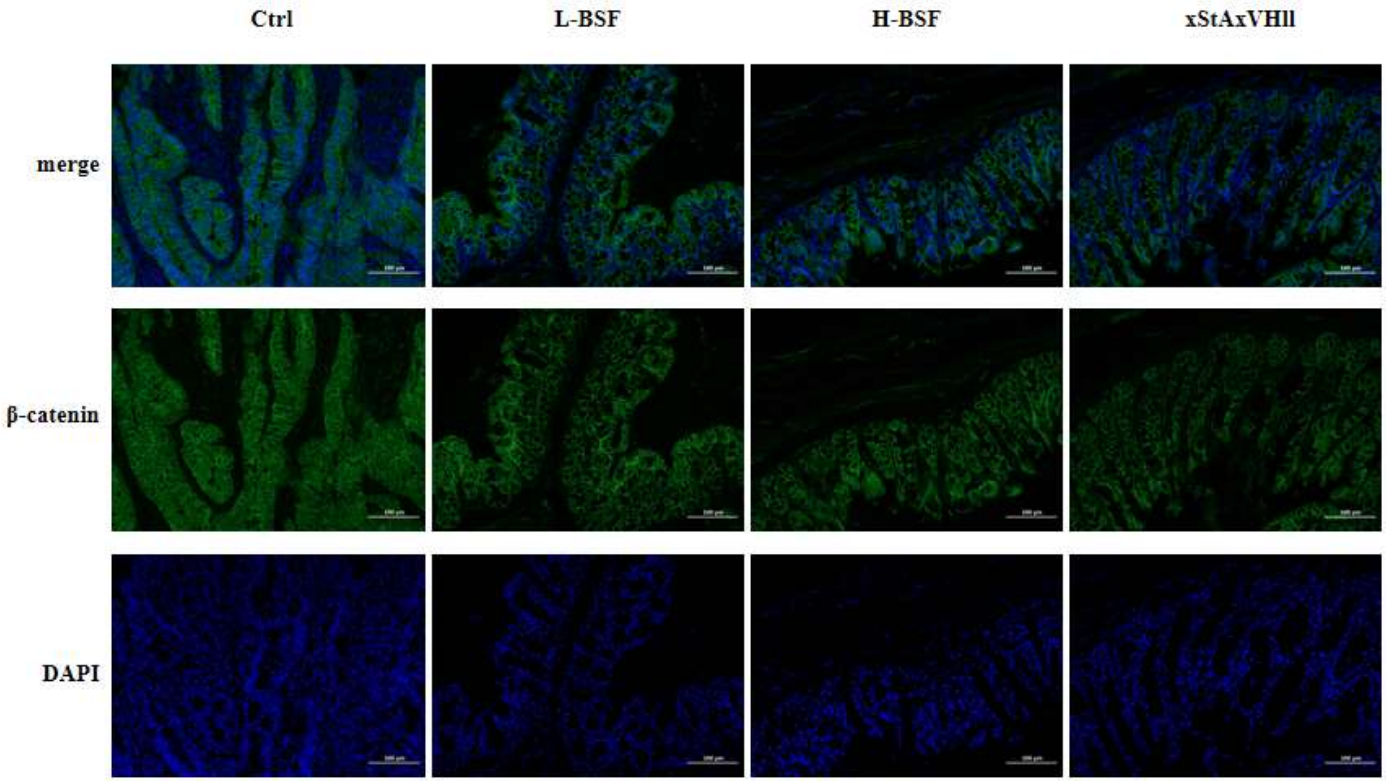

Figure 9. The effect of BuShenFang on β-catenin in the intestinal tissue of APCmin/+ mice. Ctrl indicates the control group, L-BSF represents a low dose of BSF (100 mg/kg), H-BSF denotes a high dose of BSF (200 mg/kg), and xStAxVHLL serves as the positive control.

3.7. Effect of BSF on Wnt signaling pathway-related molecules in the intestinal tissue of APCmin/+ mice

APC is a crucial factor in regulating the core protein β-catenin of the Wnt signaling pathway. It forms a degradation complex with Axin, GSK3β, and others, mediating the degradation of β-catenin after modification, thereby inhibiting the Wnt signaling pathway. When APC is deleted or mutated, the degradation of the effector protein β-catenin is obstructed, leading to its abnormal accumulation, which subsequently activates the Wnt

signaling pathway and promotes the development of colon cancer. To further investigate the changes in the Wnt signaling pathway in the intestinal tissue of APCmin/+ mice before and after BSF treatment, we employed the Western Blot method to detect the levels of APC, β-catenin, GSK-3β, p-GSK-3β, and Axin1 proteins (Figure 10). The results indicated that, compared to the Ctrl group, the APC protein levels in the intestinal tumor tissue cells of the L-BSF group, H-BSF group, and xStAxVHLL group exhibited an increasing trend ($p > 0.05$), while the levels of β-catenin, p-GSK-3β/GSK-3β, and Axin1 proteins decreased significantly ($p < 0.05$). In comparison to the xStAxVHLL group, the L-BSF group exhibited statistically significant differences in β-catenin, p-GSK-3β/GSK-3β, and Axin1 ($p < 0.001$). In the H-BSF group, β-catenin and p-GSK-3β/GSK-3β also showed statistical significance ($p < 0.01$), whereas Axin1 did not reach statistical significance ($p > 0.05$).

The downstream target genes of the Wnt/β-catenin signaling pathway, including CyclinD1, c-Myc, and COX-2, are involved in regulating apoptosis, cell cycle, and tumor metastasis. These results demonstrate that BSF can down-regulate the protein levels of β-catenin, p-GSK-3β/GSK-3β, and Axin1. Additionally, the Western Blot method was utilized to assess the protein levels of downstream target genes associated with the β-catenin pathway (Figure 10). Compared to the Ctrl group, the protein levels of β-catenin downstream target genes c-myc, CyclinD1, and COX-2 in the L-BSF group, H-BSF group, and xStAxVHLL group were significantly decreased ($p < 0.001$). These findings suggest that BSF exerts anti-cancer effects by inhibiting the Wnt signaling pathway through the upregulation of APC levels. Compared to the xStAxVHLL group, c-myc and CyclinD1 in the L-BSF group were statistically significant ($p < 0.01$), while COX-2 did not show statistical significance ($p > 0.05$). In the H-BSF group, c-myc, CyclinD1, and COX-2 did not demonstrate any statistical significance ($p > 0.05$). Overall, these findings suggest that H-BSF exerts anti-cancer effects by significantly inhibiting the Wnt signaling pathway through the upregulation of APC levels.

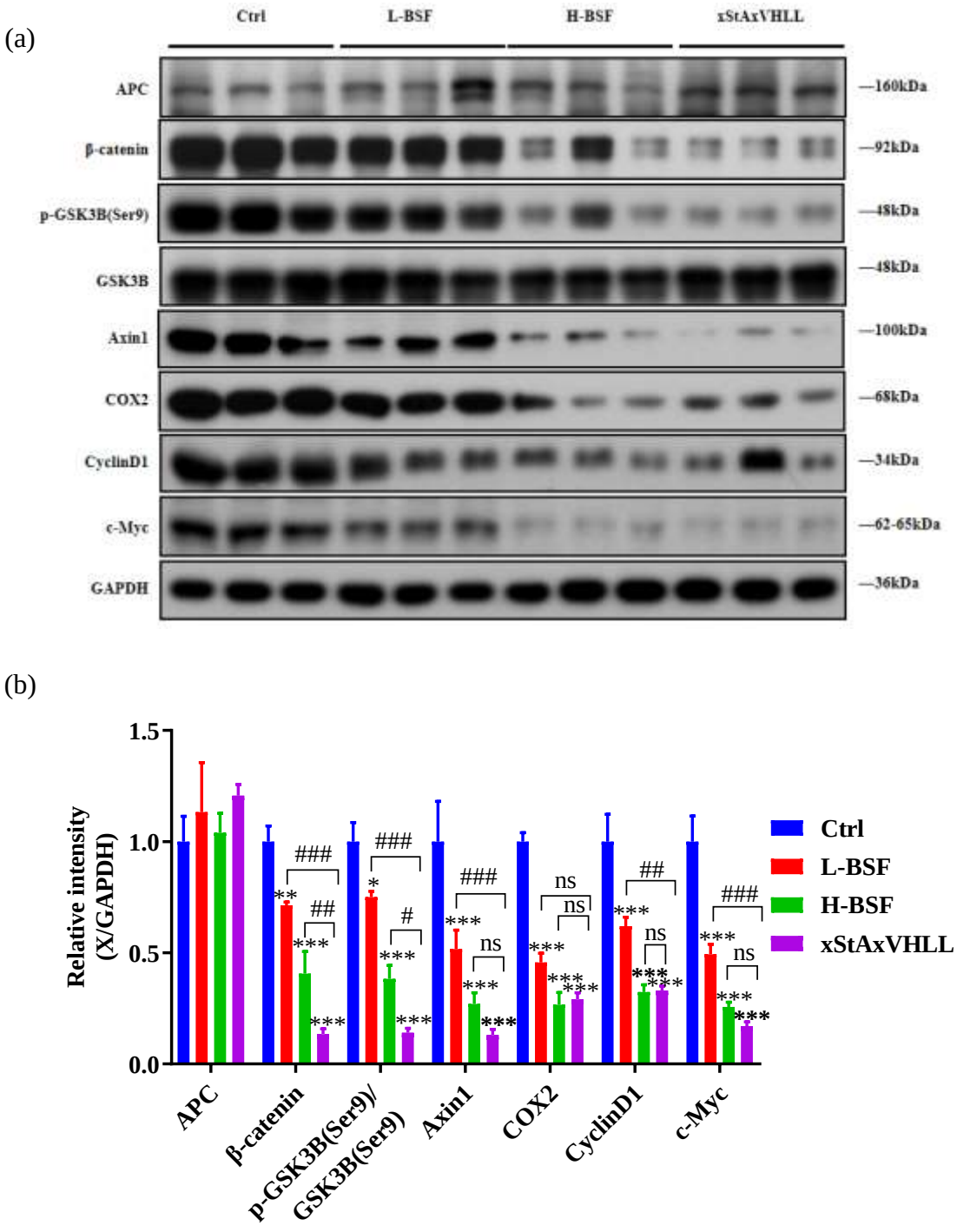

Figure 10. Effect of BSF on Wnt signaling pathway in intestinal tissue of APCmin/+ mice. Ctrl indicates the control group, L-BSF represents a low dose of BSF (100 mg/kg), H-BSF denotes a high dose of BSF (200 mg/kg), and xStAxVHLL serves as the positive control.

* vs Ctrl $p < 0.05$; ** vs Ctrl $p < 0.01$; *** vs Ctrl $p < 0.001$; ## vs xStAxVHLL $p < 0.01$; ### vs xStAxVHLL $p < 0.001$.

4. Discussion

Currently, treatment methods for CRC primarily include surgery, radiotherapy, chemotherapy, and targeted therapy. These approaches can significantly alleviate patients' symptoms, prolong survival, and enhance quality of life [14]. However, in the adjuvant treatment regimen for CRC, commonly used clinical chemotherapy agents, such as irinotecan hydrochloride, 5-fluorouracil, tigatuzumab, oxaliplatin, and cetuximab, have been associated with irreversible damage to normal tissues and organs, leading to serious adverse reactions and toxic side effects [15]. For instance, 5-fluorouracil may induce severe gastrointestinal reactions, resulting in damage to the gastrointestinal mucosa and exacerbating related symptoms [16]. Additionally, the emergence of cetuximab resistance has become a significant challenge for clinicians [17]. Consequently, the development of highly effective and low-toxicity treatment agents for CRC is crucial for enhancing therapeutic efficacy.

Recent research indicates that the pathogenesis of CRC involves multiple cascade signaling pathways, including STAT3, TGF-β, PI3K/Akt, and Wnt/β-catenin, as well as the abnormal silencing or activation of specific targets. Currently, most drugs used for CRC predominantly target only a single pathway. While it is acknowledged that a limited number of drugs currently in clinical use target a single pathway and demonstrate effective anti-CRC activity, such as immune checkpoint inhibitors, inhibiting a single signaling pathway or biological target remains challenging for the effective treatment of CRC under typical circumstances. The active components of TCM can regulate signaling molecule cascades through multiple targets, links, and effects, thereby exhibiting significant advantages in alleviating symptoms in CRC patients, enhancing their quality of life, and stabilizing lesions. Additionally, TCM can effectively prevent and treat the recurrence and progression of CRC. The efficacy of targeted therapies, including TCM with heat-clearing and detoxifying properties and its related monomers, has been demonstrated, particularly in relation to their apoptosis-inducing effects, which are primarily associated with the regulation of the STAT3 signaling pathway. Furthermore, it is evident that CRC is often preceded by the continuous infiltration of various inflammatory factors prior to its malignant transformation. The active ingredients in TCM can impede the 'inflammatory cancer' transformation process by inhibiting precancerous inflammatory responses [18]. This highlights the advantage of TCM, which aligns with the traditional philosophy of 'preventing disease before it manifests and preventing deterioration once it has occurred.

In 1990, researchers at the University of Wisconsin-Madison conducted the first genetic screening of APCMin/+ mice, identifying them as a model for studying intestinal tumorigenesis [19]. The APCMin mutation was induced through chemical mutagenesis using

N-ethyl-N-nitrosourea (ENU) [20]. This screening confirmed that the APCMin mutation leads to the spontaneous development of multiple intestinal adenomas, establishing it as a valuable model for colorectal cancer research. The APCMin/+ colorectal tumor mouse model employs an adenoviral vector carrying Cre recombinase to infect intestinal tissue, thereby activating conditional germline mutations that facilitate the formation of intestinal orthotopic colorectal adenomas [21]. In basic research, researchers often lack the genetic engineering technology required to construct such models; consequently, these models are frequently acquired from animal model companies. The APC gene serves as a tumor suppressor gene in CRC, primarily regulating β-catenin expression through the APC protein, which acts as an effector of the Wnt signaling pathway to modulate cell proliferation. In APCMin/+ mice, a mutation alters the APC gene to encode the third leucine, converting codon 850 into a stop codon. This truncation of the protein results in the loss of the APC protein's tumor suppressor function, leading to the development of colorectal tumors. Thus, mutations in the APC gene represent an early event in the progression of colorectal tumors, with most APC mutations contributing to the onset of colorectal adenomas. Targeting the APC gene may aid in the prevention and treatment of precancerous lesions associated with colorectal tumors [22-25].

Additionally, APCMin/+ mice exhibit behaviors similar to those seen in human familial adenomatous polyposis (FAP), making them an ideal model for the development of FAP-targeted drugs [26]. The APCMin/+ colorectal tumor mouse model is also valuable for research into etiology and therapeutic interventions for colorectal tumors [27, 28]. APCMin/+ mice serve as a valuable model for simulating the entire process of colorectal tumorigenesis, encompassing tumor-host interactions and the cascades of metastasis, while preserving the mice's inherent immune responses and tumor microenvironment. Consequently, this model holds significant application value in the study of tumor biology and in preclinical treatment trials. Furthermore, researchers can replicate the genes associated with colorectal tumors identified in clinical studies within the mouse genome through genetic engineering techniques, such as transgenics and gene editing, to investigate the carcinogenic effects and mechanisms of these mutations.

In this study, following the experiment, intestinal tumors from APCMin/+ mice and treated mice were selected for pathological diagnosis after hematoxylin and eosin (HE) staining. Notably, significant canceration was observed in the intestinal tissues of both the Ctrl group and the L-BSF group. It was confirmed that the selected APCMin/+ mice can spontaneously develop intestinal adenomas. However, the data indicate that the most common site for visible tumors is the small intestine, and spontaneous adenomas in APCMin/+ mice are not prone to invasion or metastasis to other tissues [29]. In this

experiment, after 11 weeks of administration, neoplastic changes in the H-BSF group and xStAxVHLL group showed significant improvement.

APCMin/+ mice spontaneously develop adenomatous polyps (APs) in the small intestine and colon due to mutations in the APC gene. The results of this study indicate that as the concentration of the BSF drug increases, both the overall number and size of tumors in the small intestine and colon decrease sequentially. Specifically, we observed that the L-BSF group inhibited APs by 53.33%, the H-BSF group inhibited APs by 66.67%, and the xStAxVHLL group inhibited APs by 46.67%. These findings showed a significant statistical difference ($p < 0.05$). These findings suggest that BSF exerts an inhibitory effect on the growth of intestinal APs in APCMin/+ mice in a dose-dependent manner. KI67 is a marker associated with proliferating cells, closely linked to mitosis, and is primarily used to identify cells in the proliferation cycle. The positive rate of KI67 is high, as more rapidly growing tumors typically exhibit poorer tissue differentiation and worse prognosis, often making them difficult to cure completely. In this study, we employed immunohistochemistry to assess the expression of KI67, a marker of cell proliferation, in adenomas across different treatment groups, revealing that the H-BSF group significantly inhibited the proliferation of mouse tumor tissues. Malignant proliferation and resistance to apoptosis are critical factors in tumorigenesis. TUNEL staining allows for the in situ detection of individual apoptotic cells or apoptotic bodies, accurately reflecting the morphological characteristics of cell apoptosis. We utilized the TUNEL method to evaluate the apoptotic effects of BSF at varying concentrations and doses, with results indicating that BSF significantly enhances the apoptosis of tumor cells. Sui et al. [30] reported that Yiyi Fuzi Baijiang San (YYFZBJS), which is composed of coix seed, aconite, and white ginger grass, includes aconite as a yang-warming and kidney-tonifying medicinal material that significantly reduces intestinal adenomatous polyps (APs) in APCmin/+ mice. Additionally, it inhibits the expression of KI67. Myricetin, an effective flavonoid compound commonly found in various fruits, vegetables, and Chinese herbal medicines, exhibits properties such as nourishing the kidneys, promoting diuresis, and facilitating dehumidification. A previous study involving APC^Min/+ mice treated with myricetin for 12 consecutive weeks found that mice receiving myricetin developed fewer and smaller intestinal polyps compared to the control group, indicating that myricetin effectively inhibited the progression of intestinal adenomatous polyps [31]. Additionally, the number of TUNEL-positive cells in small intestinal and colon adenomas increased significantly by 86.3% ($p < 0.01$), accompanied by upregulation of the pro-apoptotic Bax protein [31]. Myricetin treatment was also associated with altered β-catenin expression in both the nucleus and cytoplasm.

Signaling pathways are communication processes that mediate cellular activities through downstream genes and proteins. Disruption of these signaling processes can lead to disorders in cellular mechanisms, potentially resulting in diseases such as cancer, autoimmunity, and diabetes. Traditional Chinese medicine plays a significant role in the prevention, attenuation, efficacy, and reduction of the risk of recurrence and metastasis of CRC. The multi-target and multi-level functions of traditional Chinese medicine are increasingly recognized in the context of CRC prevention and treatment. A previous study demonstrated that the Bushen Jiedu Sanjie prescription can suppress the proliferation, metastasis, and adhesion of human colon cancer cells in a dose-dependent manner while downregulating p-STAT3 protein expression. These effects suggest its potential to reduce CRC progression by inhibiting the activation of the JAK/STAT3 signaling pathway, thereby limiting tumor invasion and metastasis [32]. Another study demonstrated that the kidney-tonifying traditional Chinese medicine Cistanche deserticola extract can inhibit the growth of human CRC transplanted tumors in nude mice. This extract upregulates the expression of HIPK2, p53, and Bax while downregulating Bcl-2. Its inhibitory effect on CRC is closely associated with the suppression of tumor cell proliferation and the promotion of apoptosis [33]. HIPK2 plays a critical role in regulating transcription, apoptosis, cell growth, and progression, functioning as both a transcriptional co-repressor and a kinase. It enhances the transcriptional activity of homologous proteins and inhibits tumor growth by activating the p53 pathway through the regulation of the Ser46 site [34-36], which is intricately linked to tumor occurrence and development.

The traditional Chinese medicine compound Bushen Jiedu Sanjie Recipe, which comprises Rehmannia glutinosa, Cistanche deserticola, August rhizome, snakeberry, Shanzi mushroom, and other ingredients, is an empirical formula developed by the Oncology Department of Shuguang Hospital affiliated with Shanghai University of Traditional Chinese Medicine. This compound is known for its functions of nourishing the kidneys, detoxifying, reducing swelling, and dispersing stagnation. Moreover, the alcohol extract of the Bushen Jiedu Sanjie prescription has been shown to inhibit the p53 signaling pathway. This dual action not only suppresses tumor growth but also inhibits the growth, cloning, and proliferation of human colon cancer HCT-116 cells by upregulating the expression levels of HIPK2 and p53 proteins in the pathway, thereby achieving therapeutic effects against CRC [37]. Verbascoside (VB) is an active compound derived from various natural Chinese herbal medicines, including Cistanche deserticola, Rehmannia glutinosa, and Artemisia annua Gansu. It exhibits anti-tumor, antioxidant, anti-inflammatory, and liver-protective properties. Zhou et al. [35] demonstrated that VB treatment significantly enhances the expression of homologous domain-interacting protein kinase 2 (HIPK2), p53, and Bax proteins in CRC

cells (HCT-116, HT-29, SW620, and LoVo). Additionally, it reduces the expression of the anti-apoptotic protein Bcl-2 in CRC cells (HCT-116, HT-29) in a time- and dose-dependent manner. The pro-apoptotic effect of VB is mitigated by the p53-specific inhibitor FPT-a. Thus, VB achieves its therapeutic effect in treating CRC by elevating the levels of HIPK2, promoting p53 phosphorylation and Bax expression, inhibiting Bcl-2 expression, and activating the HIPK2/p53 signaling pathway, ultimately increasing cell apoptosis. Icariin (ICT), a hydrolyzate extracted from Epimedium plants, has also been investigated. Treatment with ICT significantly elevates hepatocyte growth factor (HGF) levels and promotes the expression of its receptor, c-Met. Furthermore, both ICT and HGF significantly increase Bcl-2 expression while reducing the levels of Caspase-3 and Bax [38], indicating that ICT enhances the anti-apoptotic effects of mesenchymal stem cells (MSCs) by modulating the HGF/c-Met pathway.

Thus, we examined the alterations in the Wnt signaling pathway within the intestinal tissue of APCmin/+ mice before and after treatment with varying concentrations of BSF. Our findings indicated an upward trend in APC protein levels in the intestinal tumor tissue cells of the L-BSF, H-BSF, and xStAxVHLL groups ($p > 0.05$). Conversely, the levels of β-catenin, p-GSK-3β/GSK-3β, Axin1, Cyclin D1, c-Myc, and COX-2 proteins decreased significantly ($p < 0.05$). Cyclin D1, a cell cycle protein, inhibits the normal differentiation of intestinal epithelial cells, while the overexpression of c-Myc protein is detectable in mouse intestinal adenoma tissue [39]. The deletion of c-Myc leads to the blockage of intestinal adenoma formation and significantly extends lifespan. Additionally, c-Myc is known to regulate the expression of angiogenic factors and promote tumor growth [40]. Notably, nearly 80% of colon cancer tissues exhibit high levels of COX-2. Furthermore, evidence suggests that anti-COX-2 medications, such as nonsteroidal anti-inflammatory drugs like aspirin, can inhibit the progression of CRC [41]. In this experiment, the reduction in the expression of c-Myc, Cyclin D1, and COX-2 proteins due to BSF treatment was most pronounced in the H-BSF group and it is statistically significant different compared to the control group ($p < 0.05$). Additionally, berberine has been shown to protect the kidneys by alleviating various pathological changes.

Cao et al. [42] found that, compared to untreated APCmin/+ mice, the number of tumors in the proximal, middle, and distal segments of the small intestine in mice treated with 0.1% berberine was significantly reduced by 53.7%, 55.3%, and 76.5%, respectively. Berberine treatment also decreased the number of tumors of all sizes (>2 mm, 1-2 mm, and <1 mm) in the small intestine. Additionally, berberine inhibits tumor cell proliferation and increases apoptosis. Furthermore, berberine reduced the activation level of the Wnt signaling

pathway and down-regulated the expression of COX-2 in tumor cells. Thymoquinone (TQ), which is regarded as the primary compound of volatile black seed oil, possesses renal tonic and diuretic properties. APCmin/+ mice were treated with TQ over a 12-week period, during which it was observed that TQ did not affect body weight or food intake. Notably, the number of distal large intestinal polyps in mice was significantly reduced by the 9th week ($p < 0.05$). TQ induces tumor cell apoptosis and diminishes polyp growth, as evidenced by a decrease in KI67 and c-Myc positive cells following TQ treatment. Similar to berberine, TQ reduces β-catenin levels in the nucleus and lowers c-Myc expression, thereby inhibiting polyp progression in APCmin/+ mice through the regulation of Wnt signaling [43].

Zhang et al. [44] demonstrated that the expression of Cyclin D1 and c-Myc was reduced following berberine administration in APCmin/+ mice. The underlying mechanism may involve the inhibition of colon tumor formation by berberine through the suppression of Wnt/β-catenin signaling. Poria cocos is a significant medicinal and food resource known for its diuretic properties, ability to alleviate dampness, strengthen the spleen, and calm the nerves. Polysaccharides, which are among the key active components of Poria cocos, exhibit various biological activities and prebiotic effects. Treatment with Poria polysaccharides has been shown to mitigate weight loss induced by 5-FU treatment and to reduce polyp growth in APCmin/+ mice [45]. In summary, the effects of BSF on APCmin/+ mice, characterized by its ability to tonify the kidneys and strengthen yang, enhance spleen and stomach function, clear heat and detoxify, as well as eliminate carbuncles and dissipate knots, are evident in its role in controlling the number of intestinal adenomas, inhibiting carcinogenesis, reducing the proliferation of intestinal adenocarcinoma cells, promoting cancer cell apoptosis, and inhibiting the Wnt/β-catenin signaling pathway. The weight of the mice were monitored and measured throughout the study.

While the findings from this study provide compelling evidence for the tumor-inhibitory effects of BSF on APCmin/+ mice, several limitations warrant critical evaluation. First, the limited sample size and absence of a more comprehensive dose-response gradient and temporal evaluation constrain the ability to generalize findings and identify optimal therapeutic windows. Furthermore, the study primarily focused on the Wnt/β-catenin signaling pathway without exploring other potential mechanisms that might contribute to BSF's efficacy, such as modulation of immune responses or effects on tumor microenvironment factors like angiogenesis and inflammation. The reliance on immunohistochemistry and Western blotting, while valuable, precludes a more nuanced understanding of systemic effects, including serum biomarkers and cytokine profiles. Additionally, the complexity of BSF’s multi-component decoction poses challenges in

identifying specific active compounds responsible for the observed effects, which hinders the development of standardized formulations for clinical application. Future studies should consider integrating advanced molecular and multi-omics approaches to unravel alternative pathways influenced by BSF, alongside exploring its effects in combination therapies or within immune-competent tumor models for broader mechanistic insights.

The findings of this study suggest that BSF holds potential as a multi-targeted therapeutic agent for CRC, addressing limitations of conventional treatments such as severe side effects and resistance to single-target therapies. By significantly inhibiting the Wnt/β-catenin signaling pathway, a key driver of CRC progression, BSF reduces tumor proliferation and promotes apoptosis, demonstrating its capacity to modulate critical oncogenic pathways. These effects align with clinical needs for treatments that offer efficacy with reduced toxicity, particularly in patients with advanced or refractory CRC. Moreover, BSF's observed dose-dependent effects highlight its potential for precise therapeutic dosing strategies. Given the decoction's multi-component nature, it may complement existing chemotherapy or targeted therapies by addressing tumor heterogeneity and minimizing resistance through its regulation of multiple pathways, including immune modulation and anti-inflammatory actions. The integration of BSF into treatment regimens could be particularly beneficial in personalized medicine approaches, catering to patients with specific genetic or molecular profiles, such as APC mutations or hyperactive Wnt signaling. Expanding on these preclinical findings, clinical trials are essential to validate their efficacy, safety, and potential for integration into broader therapeutic contexts, including as a preventive agent in high-risk populations or an adjunct in post-operative or palliative care.

5. Conclusion

The results of this study confirm the inhibitory effect of BSF on intestinal adenoma carcinogenesis in APCmin/+ mice, potentially through the inhibition of the Wnt/β-catenin signaling pathway and the subsequent blockade of its downstream target genes, including c-Myc, cyclin D1, and COX-2. This inhibition leads to a reduction in the proliferation of colorectal adenoma cells in APCmin/+ mice while promoting apoptosis. Furthermore, it is widely acknowledged that traditional medicine offers significant advantages in the treatment of CRC, with ethnic medicine renowned both domestically and internationally for its unique therapeutic benefits. However, due to the rich and complex composition of the decoction's ingredients, standardizing pharmaceutical ingredient standards proves challenging. Additionally, numerous treatment pathways and multiple targets are involved, necessitating further experimental research into its pharmacological components and specific mechanisms

of action. This research is crucial to provide a scientific foundation for the modernization of traditional Chinese medicine and the portability of decoctions.

Acknowledgment: Animal ethics approval was obtained from Ethics Committee of Shanghai Guangde Traditional Chinese Medicine Clinic with the approval number: GD2022A-1.

Author Contributions: Conceptualization: JJ and KBL. Formal analysis: KWG, JJ, XG and HKSY. Investigation: KWG, JJ, XG and HKSY. Writing – original draft preparation: JJ, XG, RSN and HKSY. Writing – review and editing: PEK, SKL, AKJ and LCM. Validation: PEK, SKL, AKJ and LCM. Supervision: KBL. Funding acquisition: KWG and KBL.

Funding: This work was supported by the Ministry of Higher Education (MOHE) Malaysia under Fundamental Research Grant Scheme (FRGS) [FRGS/1/2021/SKK0/UOC/02/2].

Conflicts of Interest: The authors declare no conflict of interest.

References

1. Zhang RX, Li MX, Jia ZP. Rehmannia glutinosa: review of botany, chemistry and pharmacology. J Ethnopharmacol 2008; 117(2): 199-214.
2. Wang J, Wu M, Liu J, *et al*. An integrated strategy for quality control of Pseudobulbus Cremastrae seu Pleiones based on Q-marker. J Chromatogr A 2024; 1730: 465105.
3. Goh KW, Ji J, Phang HC, *et al*. Mechanistic Insights into the Inhibition of Colorectal Cancer by BuShenFang through Adenomatous Polyposis Coli Expression and Wnt/β-catenin Pathway Regulation. Prog Microbes Mol Biol 2025; 8.
4. Geraghty RJ, Capes-Davis A, Davis JM, *et al*. Guidelines for the use of cell lines in biomedical research. Br J Cancer 2014; 111(6): 1021-1046.
5. Callaway E. Contamination hits cell work. Nature 2014; 511(7511): 518.
6. ASN-0002 ATCCSDOW. Cell line misidentification: the beginning of the end. Nat Rev Cancer 2010; 10(6): 441-8.
7. Zhang L, Shay JW. Multiple Roles of APC and its Therapeutic Implications in Colorectal Cancer. J Natl Cancer Inst 2017; 109(8).
8. Hankey W, Frankel WL, Groden J. Functions of the APC tumor suppressor protein dependent and independent of canonical WNT signaling: implications for therapeutic targeting. Cancer Metastasis Rev 2018; 37(1): 159-172.
9. Jaiswal AS, Balusu R, Narayan S. Involvement of adenomatous polyposis coli in colorectal tumorigenesis. Front Biosci 2005; 10: 1118-34.
10. Zeineldin M, Neufeld KL. Understanding phenotypic variation in rodent models with germline Apc mutations. Cancer Res 2013; 73(8): 2389-99.
11. van Heemst D, den Reijer PM, Westendorp RG. Ageing or cancer: a review on the role of caretakers and gatekeepers. Eur J Cancer 2007; 43(15): 2144-52.
12. Moser AR, Pitot HC, Dove WF. A dominant mutation that predisposes to multiple intestinal neoplasia in the mouse. Science 1990; 247(4940): 322-4.
13. Pronobis MI, Rusan NM, Peifer M. A novel GSK3-regulated APC:Axin interaction regulates Wnt signaling by driving a catalytic cycle of efficient βcatenin destruction. Elife 2015; 4: e08022.

14. Rothwell JA, Murphy N, Bešević J, *et al*. Metabolic Signatures of Healthy Lifestyle Patterns and Colorectal Cancer Risk in a European Cohort. Clin Gastroenterol Hepatol 2022; 20(5): e1061-e1082.
15. Chen EX, Jonker DJ, Loree JM, *et al*. Effect of Combined Immune Checkpoint Inhibition vs Best Supportive Care Alone in Patients With Advanced Colorectal Cancer: The Canadian Cancer Trials Group CO.26 Study. JAMA Oncol 2020; 6(6): 831-838.
16. Hudita A, Radu IC, Galateanu B, *et al*. Bioinspired silk fibroin nano-delivery systems protect against 5-FU induced gastrointestinal mucositis in a mouse model and display antitumor effects on HT-29 colorectal cancer cells in vitro. Nanotoxicology 2021; 15(7): 973-994.
17. Georgiou A, Stewart A, Vlachogiannis G, *et al*. A phospho-proteomic study of cetuximab resistance in KRAS/NRAS/BRAF(V600) wild-type colorectal cancer. Cell Oncol (Dordr) 2021; 44(5): 1197-1206.
18. Sun Q, He M, Zhang M, *et al*. Traditional Chinese Medicine and Colorectal Cancer: Implications for Drug Discovery. Front Pharmacol 2021; 12: 685002.
19. Venkatachalam K, Goswami K, Madka V, *et al*. A Review of Potential Agents for Colon Cancer Interception in FAP Patients: Evidence from Preclinical Studies in APCMin/+ Mice. Targets 2025; 3(1): 4.
20. Kucherlapati MH. Mouse models in colon cancer, inferences, and implications. iScience 2023; 26(6): 106958.
21. Betzler AM, Kochall S, Blickensdörfer L, *et al*. A Genetically Engineered Mouse Model of Sporadic Colorectal Cancer. J Vis Exp 2017(125).
22. Beaugerie L and Itzkowitz SH. Cancers complicating inflammatory bowel disease. N Engl J Med 2015; 372(15): 1441-52.
23. Näthke IS. The adenomatous polyposis coli protein: the Achilles heel of the gut epithelium. Annu Rev Cell Dev Biol 2004; 20: 337-66.
24. Yamada Y, Mori H. Multistep carcinogenesis of the colon in Apc(Min/+) mouse. Cancer Sci 2007; 98(1): 6-10.
25. Taketo MM, Edelmann W. Mouse models of colon cancer. Gastroenterology 2009; 136(3): 780-98.
26. Fodde R. The APC gene in colorectal cancer. Eur J Cancer 2002; 38(7): 867-71.
27. Liu T, Guo Z, Song X, *et al*. High-fat diet-induced dysbiosis mediates MCP-1/CCR2 axis-dependent M2 macrophage polarization and promotes intestinal adenoma-adenocarcinoma sequence. J Cell Mol Med 2020; 24(4): 2648-2662.
28. Adachi S, Hamoya T, Fujii G, *et al*. Theracurmin inhibits intestinal polyp development in Apc-mutant mice by inhibiting inflammation-related factors. Cancer Sci 2020; 111(4): 1367-1374.
29. Colnot S, Niwa-Kawakita M, Hamard G, *et al*. Colorectal cancers in a new mouse model of familial adenomatous polyposis: influence of genetic and environmental modifiers. Lab Invest 2004; 84(12): 1619-30.
30. Sui H, Zhang L, Gu K, *et al*. YYFZBJS ameliorates colorectal cancer progression in Apc(Min/+) mice by remodeling gut microbiota and inhibiting regulatory T-cell generation. Cell Commun Signal 2020; 18(1): 113.
31. Li Y, Cui SX, Sun SY, *et al*. Chemoprevention of intestinal tumorigenesis by the natural dietary flavonoid myricetin in APCMin/+ mice. Oncotarget 2016; 7(37): 60446-60460.

32. Jia R, Zhang YR, Shao SY, *et al*. Bushen Jiedu Sanjie Formula reducing metastasis via regulating JAK/STAT3 signaling pathway in colorectal cancer. China Journal of Traditional Chinese Medicine and Pharmacy 2020; 35(3).
33. Zhou L, Feng Y, Jin Y, *et al*. Verbascoside promotes apoptosis by regulating HIPK2-p53 signaling in human colorectal cancer. BMC Cancer 2014; 14: 747.
34. Saul VV, Schmitz ML. Posttranslational modifications regulate HIPK2, a driver of proliferative diseases. J Mol Med (Berl) 2013; 91(9): 1051-8.
35. Calzado MA, de la Vega L, Möller A, *et al*. An inducible autoregulatory loop between HIPK2 and Siah2 at the apex of the hypoxic response. Nat Cell Biol 2009; 11(1): 85-91.
36. Nardinocchi L, Puca R, Guidolin D, *et al*. Transcriptional regulation of hypoxia-inducible factor 1alpha by HIPK2 suggests a novel mechanism to restrain tumor growth. Biochim Biophys Acta 2009; 1793(2): 368-77.
37. Feng YY, Zhou LH, Wang Y, *et al*. Bushen Jiedu Sanjie Recipe alcohol extract inhibit cell proliferation through HIPK2-p53 signaling pathway in colorectal cancer. China Journal of Traditional Chinese Medicine and Pharmacy 2017; 32(1): 4.
38. Wang L, Li S, Wang HY, *et al*. In a Rat Model of Acute Liver Failure, Icaritin Improved the Therapeutic Effect of Mesenchymal Stem Cells by Activation of the Hepatocyte Growth Factor/c-Met Pathway. Evid Based Complement Alternat Med 2019; 2019: 4253846.
39. Wang B, Tan Z, Guan F. Tumor-Derived Exosomes Mediate the Instability of Cadherins and Promote Tumor Progression. Int J Mol Sci 2019; 20(15).
40. Lu MH, Huang CC, Pan MR, *et al*. Prospero homeobox 1 promotes epithelial-mesenchymal transition in colon cancer cells by inhibiting E-cadherin via miR-9. Clin Cancer Res 2012; 18(23): 6416-25.
41. Ganduri V, Rajasekaran K, Duraiyarasan S, *et al*. Colorectal Carcinoma, Cyclooxygenases, and COX Inhibitors. Cureus 2022; 14(8): e28579.
42. Cao H, Song S, Zhang H, *et al*. Chemopreventive effects of berberine on intestinal tumor development in Apcmin/+ mice. BMC Gastroenterol 2013; 13: 163.
43. Lang M, Borgmann M, Oberhuber G, *et al*. Thymoquinone attenuates tumor growth in ApcMin mice by interference with Wnt-signaling. Mol Cancer 2013; 12(1): 41.
44. Zhang J, Cao H, Zhang B, *et al*. Berberine potently attenuates intestinal polyps growth in ApcMin mice and familial adenomatous polyposis patients through inhibition of Wnt signalling. J Cell Mol Med 2013; 17(11): 1484-93.
45. Yin L, Huang G, Khan I, *et al*. Poria cocos polysaccharides exert prebiotic function to attenuate the adverse effects and improve the therapeutic outcome of 5-FU in Apc(Min/+) mice. Chin Med 2022; 17(1): 116.